https://doi.org/10.5194/egusphere-2026-3678
Preprint. Discussion started: 7 August 2026

Multi-decadal evolution of ice-debris complexes at Muztagh Ata (Eastern Pamir) derived from Corona KH-4A and Pléiades stereo images

Zhangyu Sun[1,2,3], Tobias Bolch[3*], Daniel Falaschi[4], Atanu Bhattacharya[5,6], Lin Liu[2,7]

[1] State Key Laboratory of Water Disaster Prevention, Hohai University, Nanjing, China
[2] Department of Earth and Environmental Sciences, Faculty of Science, The Chinese University of Hong Kong, Hong Kong, China
[3] Institute of Geodesy, Graz University of Technology, Graz, Austria
[4] Instituto Argentino de Nivología, Glaciología y Ciencias Ambientales (IANIGLA), CCT Mendoza-CONICET, Argentina
[5] Department of Earth Sciences & Remote Sensing, JIS University, Kolkata, India
[6] Centre for Data Science, JIS Institute of Advanced Studies & Research, Kolkata, India
[7] Institute of Environment, Energy and Sustainability, The Chinese University of Hong Kong, Hong Kong, China

Correspondence to: Tobias Bolch (tobias.bolch@tugraz.at)

Abstract. Ice-debris complexes are glacial-periglacial transitional landforms including rock glaciers that provide important insights into geomorphological evolution and represent substantial yet overlooked water reservoirs. However, their formation and evolution remain poorly constrained. Here, we investigate ice-debris complexes at Muztagh Ata, Eastern Pamir, using historical Corona KH-4A stereo images acquired in 1967 and very-high-resolution Pléiades tri-stereo data acquired in 2013 and 2019 to reconstruct elevation changes over five decades and derive surface velocities for the recent period. Our results reveal a three-zone geomorphological organization comprising a glacier, a glacier-affected, and a periglacial zone. The glacier-affected zone exhibits extensive thermokarst features and substantial surface lowering, locally exceeding 100 m between 1967 and 2019, whereas the periglacial zone is dominated by rock glaciers with maximum surface velocities of up to 6 m/yr. These zones occupy approximately 39.4 km², 6.5 km², and 9.4 km², respectively. Despite their considerably smaller area, the glacier-affected and periglacial zones experienced ice volume losses comparable to those of the glacier zone during 1967–2019. Our observations suggest that multiple evolutionary pathways can operate simultaneously within a single ice-debris complex. Glacier-affected landforms may progressively evolve into rock glaciers, whereas debris-covered glaciers may advance onto or become embedded within pre-existing rock glaciers. This study provides new insights into the evolution of ice-debris complexes and highlights the need to incorporate these landforms into glacier inventories and hydrological models for water resource assessments in High Mountain Asia and other mountainous regions on Earth.

https://doi.org/10.5194/egusphere-2026-3678
Preprint. Discussion started: 7 August 2026

1 Introduction

Mountain regions host a wide variety of landforms composed of mixtures of ice and debris including debris-covered glaciers, ice-cored moraines, and rock glaciers, which reflect the combined influence of glacial and periglacial processes (Monnier and Kinnard, 2017; Jones et al., 2019a; Herreid and Pellicciotti, 2020; Zalazar et al., 2020). These landforms are often geomorphologically complex because their formation and evolution are governed by interactions between long-term ice deformation, sediment supply, permafrost and climatic forcing (Haeberli et al., 2006; Gärtner-Roer et al., 2022; Knight and Harrison, 2014). To describe this complexity, Bolch et al. (2019) introduced the term ice-debris complex, referring to "complex debris landforms that are close to glaciers and composed of several elements such as rock glaciers in various stages of activity, ice-cored moraines, and debris-covered dead-ice bodies that show no signs of movement." This term was used by several studies since then to describe similar complex landforms elsewhere (e.g. Zhou et al., 2022; Blöthe et al., 2021). Ice-debris complexes usually exhibit a spatial transition from debris-covered ice, commonly bearing thermokarst depressions and meltwater ponds, to a rock glacier-like landform with ridge-and-furrow topography and steep frontal slopes (Bolch et al., 2019).

Understanding ice-debris complexes is important for several reasons. First, these landforms occupy key transitional zones between glacial and periglacial environments and therefore provide insights into the geomorphological evolution of high mountain terrain (Bolch et al., 2019; Haeberli et al., 2024; Wee et al., 2024). Second, they play a significant role in sediment transport, debris storage and release, linking sediment cascades from glaciers to downstream geomorphic systems such as alluvial fans, outwash plains, and valley floors and can be a source of hazardous debris flows (Lugon and Stoffel, 2010; Cusicanqui et al., 2021; Munroe et al., 2024). Third, the partial or complete preservation of buried ice has important hydrological implications, especially for regions where meltwater from debris-mantled ice bodies contributes to local water resources (Janke et al., 2017; Bolch et al., 2019; Jones et al., 2019b; Harrison et al., 2021, 2024; Villarroel et al., 2022).

Earlier studies in the European Alps suggested that the occurrence of ice-debris complexes is driven by Holocene glacier oscillations and debris supply from surrounding rockwalls (Haeberli, 2005). Long-term monitoring at Gruben and Ritord sites in the Swiss Alps has elucidated how creeping permafrost, buried glacier ice, debris-covered glaciers, and former glacier margins interact physically over decades (Kääb et al., 1997; Gärtner-Roer et al., 2022; Wee et al., 2024, 2026). Other studies in the dry Andes of Argentina and Chile also identified complex transition zones where glacier forefields frequently host composite landforms characterized by multi-phase development (Monnier et al., 2014; Monnier and Kinnard, 2015, 2017; Janke et al., 2017; Villarroel et al., 2022). Similarly, research in the Tien Shan revealed that ice-debris complexes consist of coexisting, spatially connected elements, including ice-cored moraines, dead-ice bodies, and active or relict rock glaciers (Bolch et al., 2019; Blöthe et al., 2021; Wood et al., 2026). Recent frameworks describe this evolution through paraglacial transition models, where landscape responses may modulate glacier sensitivity to climate change (Harrison et al., 2025). However, despite the widespread presence of ice-debris complexes, most mountain ranges in High Mountain Asia,

https://doi.org/10.5194/egusphere-2026-3678
Preprint. Discussion started: 7 August 2026

including the Pamir, lack long-term records of elevation change and spatially resolved surface motion, limiting our understanding of their long-term evolution.

In this study, we investigate ice-debris complexes in the Muztagh Ata massif, Eastern Pamir, using historical and contemporary satellite stereo images. By combining declassified Corona KH-4A stereo imagery acquired in 1967 with very-high-resolution contemporary Pléiades tri-stereo imagery acquired in 2013 and 2019, we quantified long-term elevation changes and derived surface velocity fields. These datasets were further integrated with geomorphological observations to delineate distinct landform units within the ice-debris complexes and characterize their spatial organization. The objectives of this study are to (i) quantify the long-term elevation changes and recent surface velocities of ice-debris complexes, (ii) investigate their geomorphological characteristics and evolutionary pathways, and (iii) assess their potential hydrological significance as solid water reservoirs. By linking multi-decadal elevation changes, surface velocities, and geomorphological mapping, this study provides the first comprehensive assessment of ice-debris complexes in the Tibet–Pamir region and offers new insights into glacier–permafrost interactions in High Mountain Asia and beyond.

2 Study area

The Muztagh Ata massif (38.10–38.40° N, 75.00–75.35° E) is in the eastern Pamir Mountains, Xinjiang province, western China (Fig. 1a), at the north-western margin of the Tibetan Plateau. Mount Muztagh Ata rises to a maximum elevation of 7,546 m a.s.l. and with surrounding terrain extending from approximately 3,500–4,000 m a.s.l. up to the peak (Falaschi et al., 2023). The climate is cold and semi-arid, dominated by mid-latitude westerlies rather than the Indian monsoon, making the region among the driest and coldest zones at mid-latitudes (Zhou et al., 2014). Observational data (2009–2016) from a weather station at ~3,650 m a.s.l. recorded a mean annual and summer (June–August) air temperature of ~0.34 °C and ~10.06 °C respectively and mean annual precipitation of ~154 mm (Yang et al., 2024). No direct ground surface temperature measurements exist, but modelling results show that permafrost is likely even in the lower parts of the glaciers and the ice-debris complexes (Fig. 1a)

Muztagh Ata massif has a substantial glacierized area with 128 glaciers covering ~377 km^2 (RGI 7.0 Consortium, 2023) and is included in the wider area of Karakoram Anomaly, a phenomenon where glaciers in this region remained stable or even gained mass despite global warming trends (Holzer et al., 2015; Kääb et al., 2015; Lv et al., 2020). Previous glacier-focused studies show that the glacier area change in the massif was minimal (–3.84±0.8 km^2 over 1967–2019), with mass balance changes near zero or slightly negative (–0.06±0.07 m w.e.a^{-1} over 1967–2019), indicating a nearly balanced glacier system over five decades (Bhattacharya et al., 2021). However, the most recent data showed that glaciers in this region including Eastern Pamir have shifted toward accelerated mass loss, suggesting the possible finalization of the anomaly (Berthier and Brun, 2019; Hugonnet et al., 2021; Falaschi et al., 2023). Given the high relief, cold climate, and abundant presence of valley glaciers, debris-covered tongues, and ice-debris complexes, Muztagh Ata represents an ideal study area for glacier–periglacial interactions in the transition zone between the Pamir and the Tibetan Plateau.

https://doi.org/10.5194/egusphere-2026-3678
Preprint. Discussion started: 7 August 2026

Here, we focus on four ice-debris complexes located in the southern part of Muztagh Ata (Fig. 1b, Table S1), which extend further downvalley from the extent included in the RGI v7.0 or GAMDAM glacier inventory (RGI 7.0 Consortium, 2023). These complexes exhibit a wide range of geomorphological features, including surging-affected glacier tongues and various activity stages of rock glaciers, making them highly representative of the glacier–periglacial transitional landforms in Eastern Pamir. Moreover, these complexes are fully covered by both available historical Corona and contemporary Pléiades images, allowing for multi-decadal analysis.

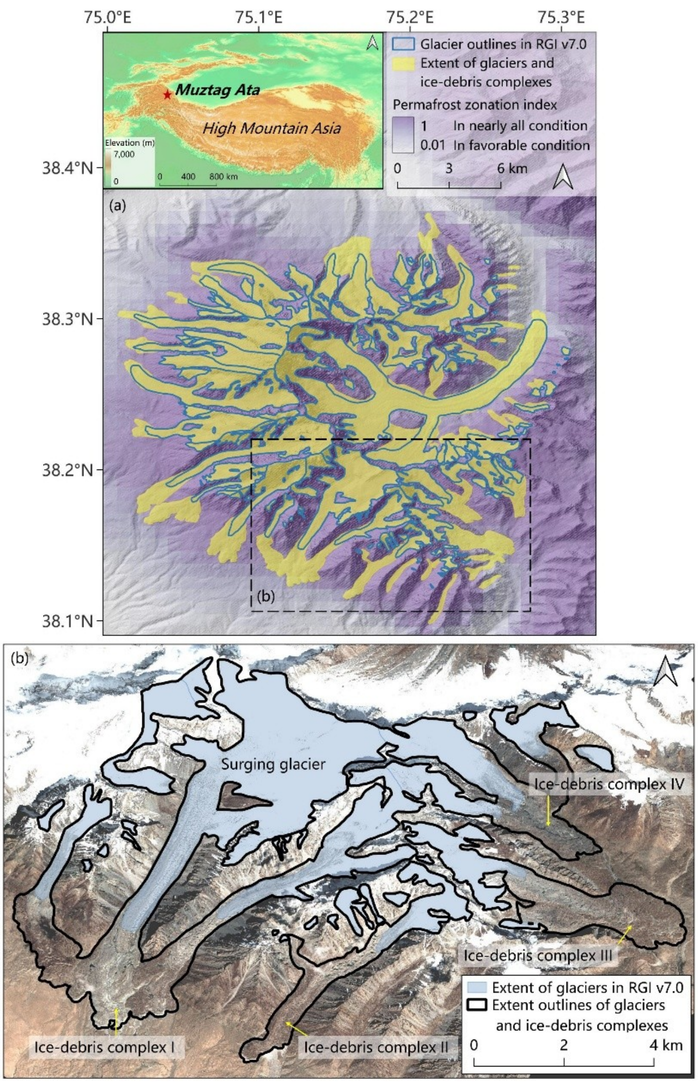

Figure 1: (a) Coverage by glaciers and ice-debris complexes in the Muztagh Ata. The glacier outlines are from the Randolph Glacier Inventory (RGI v7.0, RGI 7.0 Consortium, 2023). Permafrost zonation index map is from Gruber (2012). The background is the Copernicus Digital Elevation Model (European Space Agency, 2024). (b) The investigated four ice-debris complexes in the southern Muztagh Ata and the upslope connected glaciers in the corresponding valleys. The background is a pansharpened true color composite of Pléiades satellite imagery (5 Sep 2019, 11 Sep 2019 © CNES and Airbus DS (2019), all rights reserved).

https://doi.org/10.5194/egusphere-2026-3678
Preprint. Discussion started: 7 August 2026

3 Data and Methods

To study the elevation changes and surface velocities of the ice-debris complexes, we processed declassified Corona KH-4A and Pléiades images to generate historical and contemporary Digital Elevation Models (DEMs) and orthoimages (Sects. 3.1 and 3.2), which were used to generate elevation changes (Sect. 3.3) and surface velocity fields (Sect. 3.4). Based on the generated dataset, we delineated boundaries to differentiate units and performed geomorphological characterization (Sect. 3.5).

3.1 Processing of declassified Corona images

Two stereo pairs of Corona KH-4A images acquired on 10 August 1967 (Table 1) were used to generate historical DEMs using the Remote Sensing Software Graz (RSG) v.24.0.0 (cf. Goerlich et al., 2017; Bhattacharya et al., 2021). The subset images downloaded from USGS archive were first stitched to form complete strips. To improve DEM generation, image contrast was enhanced in ERDAS IMAGINE using a 3×3 local adaptive filter and histogram equalization of both forward and backward strips. While the adaptive filter enhances local spatial contrast, histogram equalization improves global radiometric contrast, facilitating more robust stereo correlation. Landsat panchromatic images (spatial resolution 15 m) and Copernicus DEM (European Space Agency, 2024) were used to collect 30–50 ground control points using the integrated point measurement tools of RSG. These points were used to calibrate a Corona-tailored image distortion model based on a modified collinearity equation (Sohn et al., 2004). Then, tie points were generated using a matching-based automated method to co-register the stereo pairs, followed by polynomial rectification and epipolar registrations. Image matching was performed in five pyramid-based levels to predict disparity maps (Goerlich et al., 2017). Quality and back-matching threshold filters of 0.6 and 0.9 pixels, respectively, were used to identify and remove mismatch pixels. Finally, the filtered disparity maps were converted to height maps, which were used to generate 5 m spatial resolution DEM in the WGS84 ellipsoidal coordinate system.

Table 1: Details about the remotely sensed data used in this study.

Sensors	Scenes/Product ID	Date	Spatial resolution (m)
Corona KH-4A	DS1043-1039DF072 DS1043-1039DA072 DS1043-1039DA073	10-08-1967	4
Pléiades	DS_PHR1B_201306190558223_FR1_PX_E075N38_0106_02977 DS_PHR1A_201306200550211_FR1_PX_E075N38_0306_03390	19-06-2013 20-06-2013	0.5
	DS_PHR1B_201909050554111_FR1_PX_E075N38_0306_03316 DS_PHR1A_201909110558233_FR1_PX_E075N38_0106_02862	05-09-2019 11-09-2019	0.5

https://doi.org/10.5194/egusphere-2026-3678
Preprint. Discussion started: 7 August 2026

3.2 Processing of Pléiades images

We generated DEMs from Pléiades tri-stereo panchromatic imagery acquired on 19 June 2013, 20 June 2013, 5 September 2019, and 11 September 2019 (Table 1) using the Ames Stereo Pipeline (ASP v3.1.0), a NASA-developed software suite later refined by Shean et al. (2016). Initial orthorectification of the stereo images at 0.5 m resolution was performed using the Copernicus DEM (European Space Agency, 2024). Stereo matching employed the Semi-Global Matching (SGM) algorithm (Hirschmüller, 2008) with a 7×7-pixel correlation window (Shean et al., 2020). To reduce artifacts in the disparity maps, SGM-based disparity filters (Shean et al., 2016) were applied, followed by refinement of valid disparity pixels using a Bayesian Expectation-Maximization weighted affine adaptive window correlator (Nefian et al., 2009). Stereo triangulation was performed using the rational polynomial coefficient (RPC) sensor model (Grodecki and Dial, 2003). The final DEMs were sampled at 2 m spatial resolution in the WGS84 ellipsoidal coordinate system. No ground control points were used during DEM extraction. To reduce potential systematic offsets, all DEMs were subsequently co-registered before elevation change analysis (Berthier et al., 2024; Falaschi et al., 2023).

3.3 Calculation of elevation changes

We used the xDEM package to co-register multi-temporal DEMs and calculate Differences of DEMs (DoDs). xDEM is a Python library designed for quantitative analysing DEMs, providing an intuitive object-based Application Programming Interface that facilitates user-friendly elevation data analysis (Hugonnet et al., 2024). A 200 m buffer was generated around each ice-debris complex to approximate surrounding stable terrain. Instead of processing the full DEMs, we restricted the analysis to each ice-debris complex and the terrain within its 200 m buffer. We acknowledge that the buffered area may locally include terrain that is not strictly stable, such as steep slopes, or areas covered by loose debris. However, the buffer was chosen to balance proximity to the ice-debris complex with sufficient spatial coverage, under the assumption that most areas within this distance represent relatively stable ground compared to the actively deforming ice-debris complex.

The 2013 Pléiades DEM was used as the reference DEM for co-registration of all other DEMs. Co-registration was carried out following Nuth and Kääb (2011) to correct horizontal and vertical shifts. After applying the Nuth and Kääb method, deramping was performed using a two-dimensional polynomial fitting approach to remove residual large-scale trends. Additionally, block co-registration was applied to reduce remaining non-linear artefacts. For Corona KH-4A co-registration, both DEMs were resampled to a common spatial resolution of 5 m, whereas Pléiades DEMs were co-registered at a spatial resolution of 2 m.

The buffer areas of stable terrain used for co-registration contain steep slopes where DEMs are prone to errors, which can degrade the accuracy of DEM differencing. To improve the DoD quality, we removed pixels within the buffer areas whose absolute elevation differences exceeded 20 m for the 2013 Pléiades–1967 Corona KH-4A pair and 2 m for the 2019–2013 Pléiades pair.

https://doi.org/10.5194/egusphere-2026-3678
Preprint. Discussion started: 7 August 2026

Analysis of DoD within the buffer areas surrounding the ice-debris complexes revealed Normalized Median Absolute Deviations (NMAD) of 4–6 m for 1967–2013 and 0.7–0.9 m for 2013–2019 (Table S2). NMAD can serve as a measure of the uncertainty in elevation change (Höhle and Höhle, 2009; Dehecq et al., 2016; Bolch et al., 2019), and the observed values are in line with other studies using similar input DEM data (e.g., Belart et al., 2017; Falaschi et al., 2023).

3.4 Generation of surface velocity fields

We used the vmap package to derive surface velocity fields for the ice-debris complexes from the orthorectified Pléiades image pair acquired in 2013 and 2019. This package utilizes the ASP image correlator to efficiently perform feature tracking between two time-separated scenes (Shean et al., 2020). Prior to feature tracking, the input images were co-registered using AROSICS, which is an automated and robust open-source tool for multi-sensor satellite image co-registration (Scheffler et al., 2017). Feature tracking was then conducted using vmap with a kernel size of 51 pixels. While a smaller kernel is more sensitive to fine-scale displacements, it may fail to capture high-velocity regions. Conversely, a larger kernel can better capture fast movements but results in a less detailed velocity field. After testing various kernel sizes, we determined that a 51-pixel kernel provided the optimal balance.

The NMAD of stable terrain within buffer areas can serve as a measure of surface velocity uncertainty (Table S3). The median plus three times of NMAD was used as a threshold to distinguish clearly from non-clearly detectable movement: rock glaciers with median velocities exceeding this threshold were classified as “rock glacier with clearly detectable velocities”, whereas those below the threshold were categorized as “rock glacier without clearly detectable velocities”.

3.5 Geomorphological mapping

We produced geomorphological maps through an integrated analysis of orthorectified Pléiades images, surface elevation change maps, and surface velocity fields. Based on these datasets, we differentiated various units within the ice-debris complexes, including debris-free and debris-covered glaciers, ice-cored moraines, debris-covered dead ice bodies, and rock glaciers. The separation of these units was guided by a combination of geomorphological, elevation change, and surface velocity criteria (Table 2). In addition, we mapped the landforms surrounding the ice-debris complexes, including adjacent talus, bedrock, and mountain ridges. We followed the geomorphological mapping legend developed by the University of Lausanne (Lambiel et al., 2013), which has been successfully applied in other high-mountain environments (Lambiel et al., 2016) and for mapping ice-debris complexes (Bolch et al., 2019).

Debris-covered glacier parts were included in the analysis. The upslope boundary of the analysis area was defined based on debris-free glacier extents derived from Sentinel-2 imagery (Paul et al., 2016; Fig. S1). However, the transition between debris-free and debris-covered glaciers is often ambiguous (Zalazar et al., 2020) (e.g., ice-debris complex II). For consistency and simplicity, a straight-line boundary was adopted to define the upslope limit of the analysis area as also suggested for glacier and rock glacier inventories with uncertain boundaries (RGI 7.0 Consortium, 2023; Brardinoni et al., 2026).

https://doi.org/10.5194/egusphere-2026-3678
Preprint. Discussion started: 7 August 2026

Table 2: The geomorphological, elevation change, and surface velocity criteria to distinguish different ice-debris complex units.

Zone	Landform	Geomorphological criteria	Elevation change criteria	Surface velocity criteria
Glacier zone	Debris-free glacier	Exposed ice, supraglacial crevasses, lack of debris mantle	Pronounced surface lowering, substantial gains in surging units	Rapid flow in surging units
	Debris-covered glacier	Debris mantle, supraglacial ponds, thermokarst depressions, ice cliffs	Pronounced surface lowering, localized gains during surging	Rapid flow in surging units
Glacier-affected zone	Ice-cored moraine	Ridge-like morphology, chaotic surface texture, chaotic thermokarst features	In most cases median surface lowering larger than NMAD over stable terrain	Irregular deformation to stagnant
	Debris-covered dead ice body	Irregular topography, extensive thermokarst depressions and meltwater ponds	Pronounced and widespread surface lowering, median surface lowering larger than NMAD over stable terrain	Stagnant
Periglacial zone	Rock glacier with significant movement	Coherent viscous flow patterns, well-developed ridge-and-furrow topography, steep frontal slopes and distinct lateral margins	Characteristic elevation gains at the front indicating advance, median surface lowering smaller than NMAD over stable terrain	Clearly detectable movement with median velocity above detection threshold
	Rock glacier without significant movement	Similar morphology to active rock glaciers but often more subdued	Negligible elevation change, median surface lowering smaller than NMAD over stable terrain	No clearly detectable movement with median velocity below detection threshold

4 Results

This section first describes the geomorphological units along with their classifications (Sect. 4.1) and then presents elevation changes (Sect. 4.2) and surface velocities (Sect. 4.3).

4.1 Geomorphological units

The unit separations and classifications are presented first to serve as an organizational framework, although they were ultimately derived from the integrated analysis of surface geomorphology, elevation changes, and surface velocities. Complexes I–IV were subdivided into 12, 10, 12, and 10 geomorphological units, respectively. These units were delineated

https://doi.org/10.5194/egusphere-2026-3678
Preprint. Discussion started: 7 August 2026

to represent internally consistent geomorphological entities that share similar surface characteristics, elevation-change signatures, and velocity patterns according to the criteria summarized in Table 2. The units were grouped into three major zones: a glacier zone, a glacier-affected zone, and a periglacial zone (Fig. 2 and Table 3). The glacier (including debris-free glaciers), glacier-affected, and periglacial zones occupy approximately 39.4 km^2, 6.5 km^2, and 9.4 km^2, respectively.

Complexes I, II, and IV are dominated by periglacial rock-glacier units, whereas Complex III contains a larger proportion of glacier-affected units. For simplicity, units are referred to using a combined naming system, where I-2 denotes Unit 2 of Complex I and III-1 denotes Unit 1 of Complex III. Surge-type debris-free or debris-covered glaciers were identified in I-2, III-1, IV-1, and IV-2, while debris-covered dead ice bodies occur in I-4, III-2, and IV-3. Rock glaciers with clearly detectable velocities were identified in I-5, II-5, III-8, III-9, IV-6, and IV-7, whereas the remaining rock glacier units exhibited no clearly detectable movement during the observation period.

Table 3: Geomorphological units and their classifications of different ice-debris complexes.

Ice-debris complex ID		I	II	III	IV
Glacier zone	Debris-free glacier	N/A	N/A	N/A	1
	Debris-covered glacier	1–3	1–4	1	2
Glacier-affected zone	Debris-covered dead ice body	4	N/A	2	3
	Ice-cored moraine	N/A	N/A	3–7	4, 5
Periglacial zone	Rock glacier with clearly detectable velocities	5	5	8, 9	6, 7
	Rock glacier without clearly detectable velocities	6–12	6–10	10–12	8–10

https://doi.org/10.5194/egusphere-2026-3678
Preprint. Discussion started: 7 August 2026

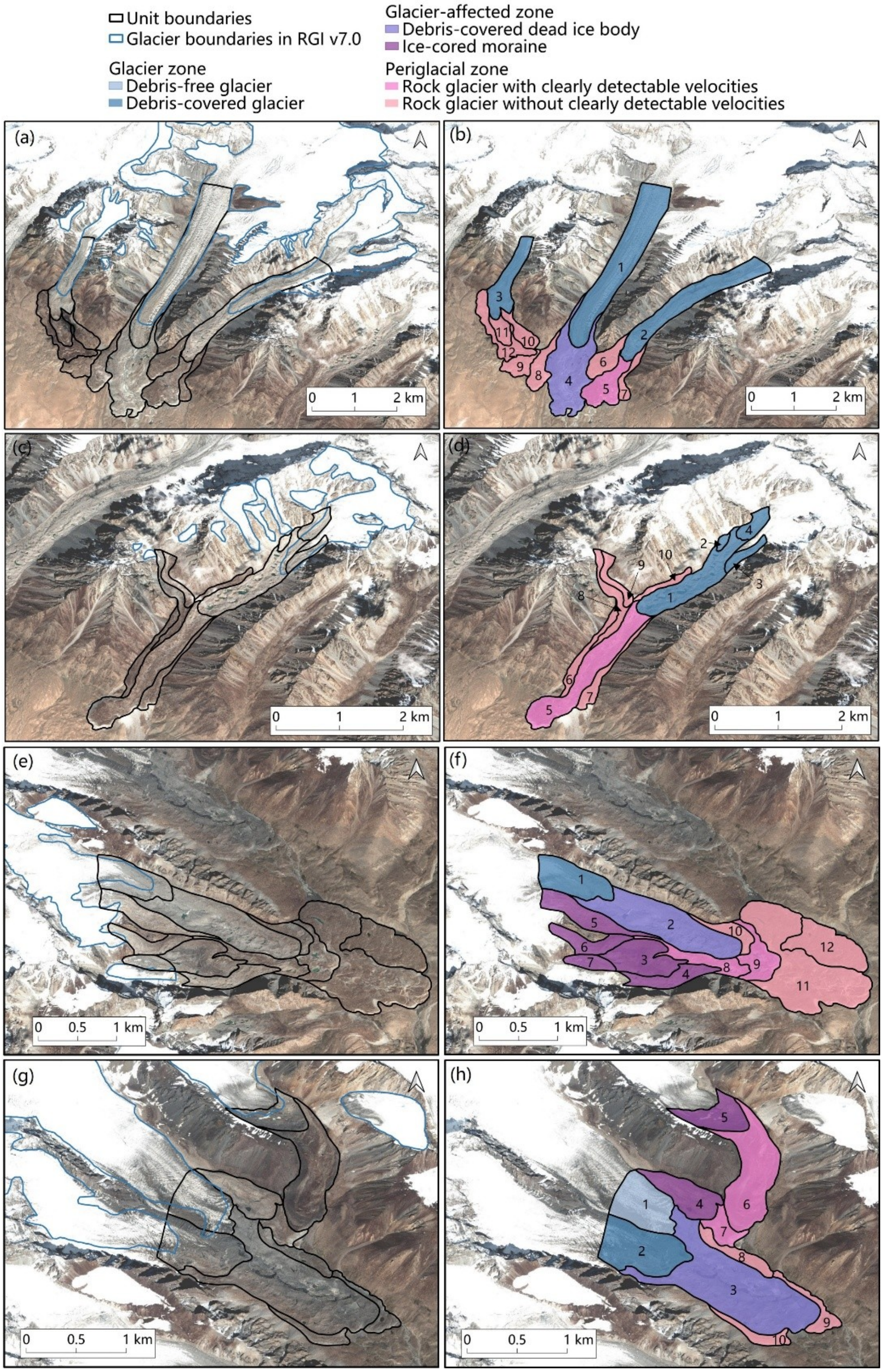

Figure 2: Geomorphological units of ice-debris complex (a–b) I, (c–d) II, (e–f) III, (g–h) IV.

https://doi.org/10.5194/egusphere-2026-3678
Preprint. Discussion started: 7 August 2026

4.2 Elevation changes

The DEM differencing between 1967 and 2013 reveals pronounced surface lowering in the debris-covered dead ice body units (I-4, III-2, and IV-3) with median lowering ranges from 10 to 20 m, and the local maxima between 60 and 100 m (Figs. 3a,e,g, S2a,c,d and Table S4). The largest surface lowering occurs in the upper-central sectors of these units. The debris-covered glacier units of Complexes I and II (I-2 and II-1) also exhibit widespread surface lowering with a median lowering of ~10 m and local maxima between 40 and 50 m (Figs. 3a,c, S2a,b, and Table S4). Pronounced elevation gains are observed on the lower part of I-1 with the maximum gain of almost 60 m caused by glacier surging (Figs. 3a and S2a). Other units remain relatively stable without pronounced surface lowering or elevation gains (Fig. S2 and Table S4). Slight elevation gains at the fronts of some rock glacier units (e.g., I-5 and II-5) are observed (Figs. 3a,c, and S2a,b), with maximum gains between 30 and 40 m (Table S4).

The high-resolution surface elevation changes derived from Pléiades 2013–2019 data reveal finer-scale spatial patterns. Pronounced surface lowering is also observed in the debris-covered dead ice body units of III-2 and IV-3, with maximum lowering between 40 and 50 m (Figs. 3f,h, S3c,d, and Table S4). Heterogeneous elevation changes are evident in the debris-covered glacier units I-2 and II-1, with the maximum elevation losses of 30–60 m, and maximum elevation gains of 10–60 m (Figs. 3b,d, S3a,b, and Table S4). More regular and transverse bands of alternating elevation gains and lowering are observed on rock glacier units, such as I-5 and II-5 (Figs. 3b,d, and S3a,b). These two units show the maximum elevation changes of ±10 m (Table S4). Pronounced elevation gains are observed on the surge-type debris-free/covered glacier units (I-1, III-1, IV-1, and IV-2) with maximum elevation gains between 25 and 70 m (Figs. 3b,f,h, S3a,c,d, and Table S4).

The elevation change rates exhibited notable differences between the two observation periods (Figs. 3, 4, and Table S5). For example, II-1 exhibits more pronounced elevation change rates during 2013–2019 (Median = −0.34 m/yr) than during 1967–2013 (Median = −0.20 m/yr) (Figs. 3c,d, and 4b). Median elevation change rates of I-4, III-2, and IV-3 were −0.19, −0.36, and −0.48 m/yr, respectively, during 1967–2013, compared to −0.08, −0.10, and −0.10 m/yr during 2013–2019 (Figs. 3a,b,e–h and 4a,c,d).

https://doi.org/10.5194/egusphere-2026-3678
Preprint. Discussion started: 7 August 2026

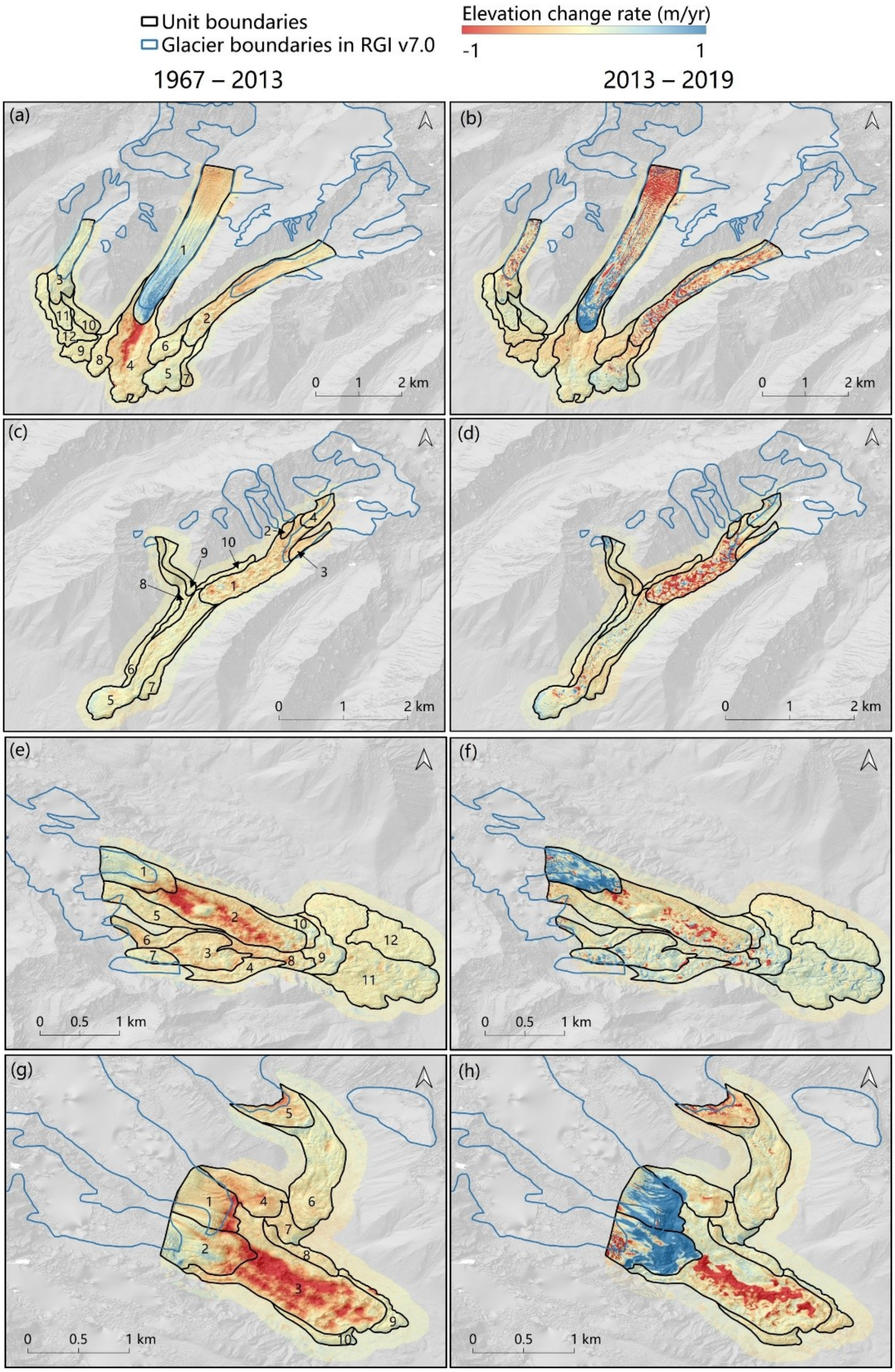

240 **Figure 3: Surface elevation change rates of ice-debris complexes I–IV for the periods of (first column) 1967–2013 and (second column) 2013–2019.**

https://doi.org/10.5194/egusphere-2026-3678
Preprint. Discussion started: 7 August 2026

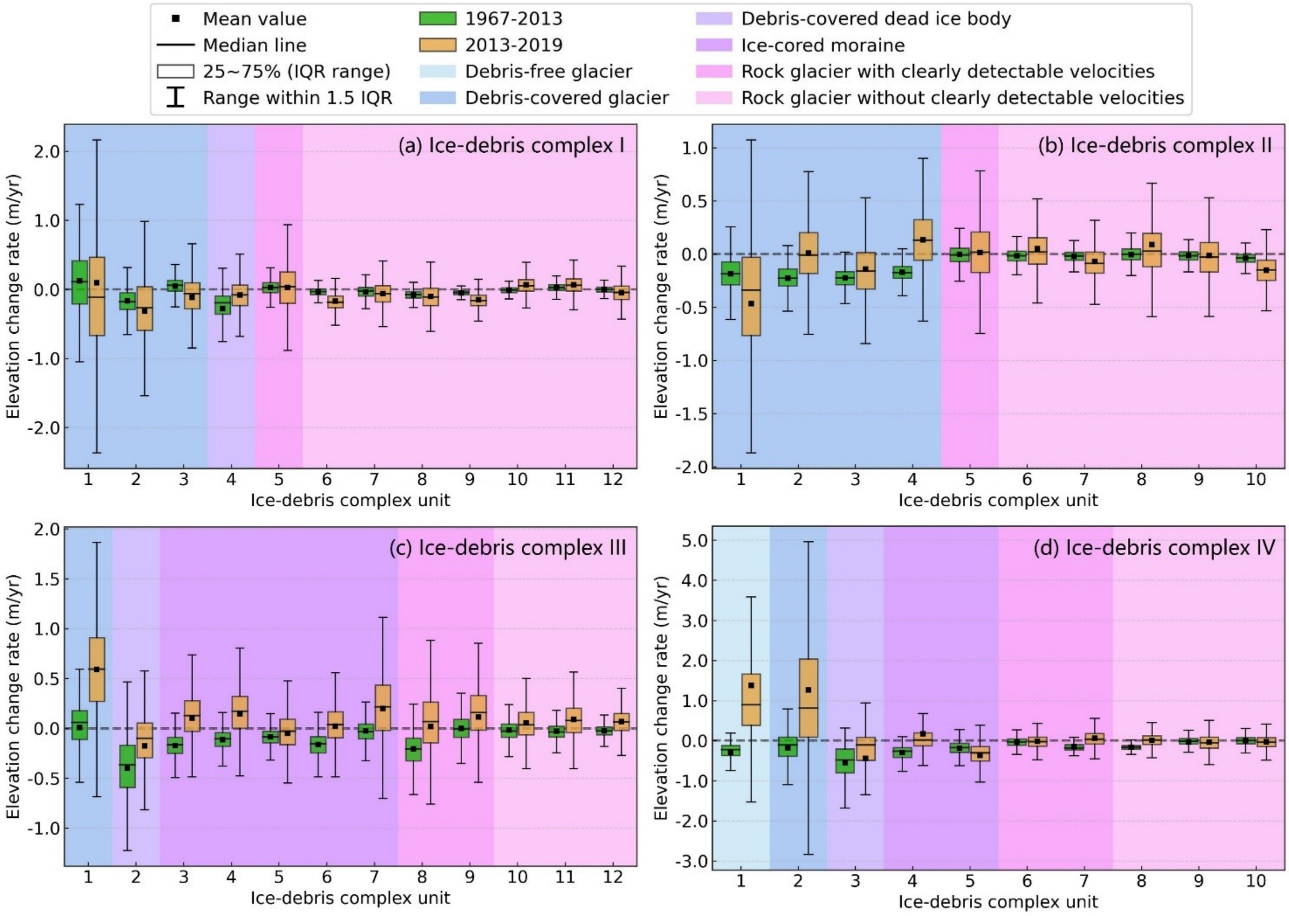

Figure 4: Distribution of elevation change rates for ice-debris complex (a) I, (b) II, (c) III, and (d) IV in the period of 1967–2013 and 2013–2019. IQR: Interquartile Range.

4.3 Surface velocities

Feature tracking reveals clearly detectable surface velocities in some rock glacier units of the ice-debris complexes (Figs. 5, 6, and Table S5). The fastest-moving rock glacier units are I-5 and II-5, which exhibit median velocities of ~2 m/yr and maximum velocities exceeding 6 m/yr (Figs. 5a,b and 6a,b). In contrast, the other rock glacier units with clearly detectable movement (III-8, III-9, IV-6, and IV-7) exhibit median velocities ranging from 0.8 to 1.5 m/yr (Figs. 5c,d and 6c,d). Other units that display geomorphological characteristics typical of rock glaciers remain relatively stable, with median velocities below the detection thresholds defined in Sect. 3.4 (e.g., I-6 to I-12; Figs. 5a, 6a, and Table S5).

https://doi.org/10.5194/egusphere-2026-3678
Preprint. Discussion started: 7 August 2026

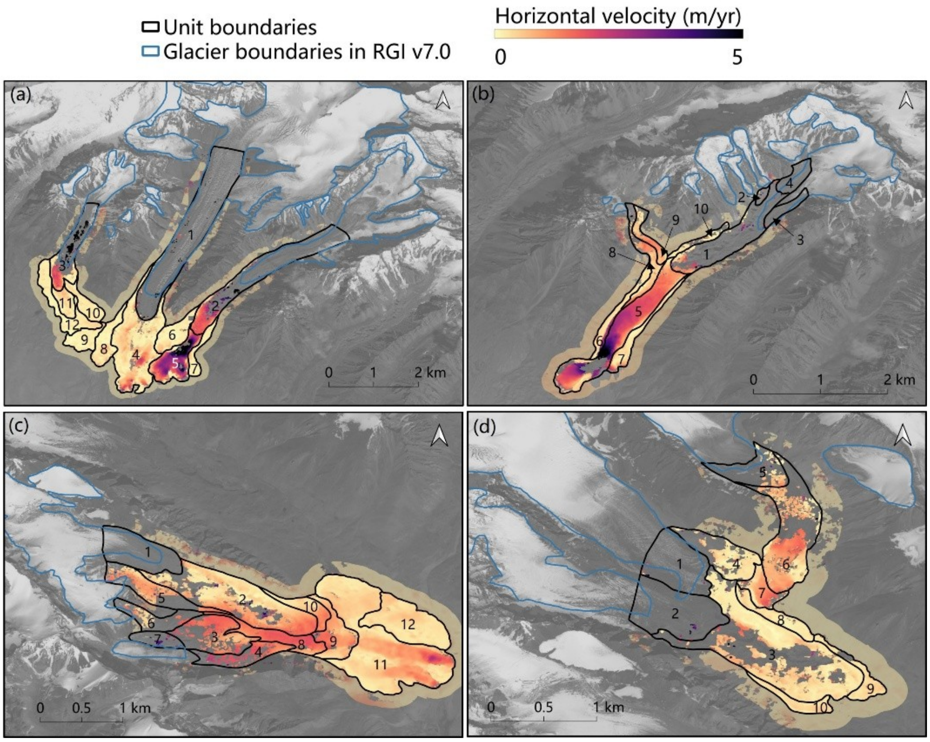

Figure 5: Surface velocity fields during 2013–2019 of ice-debris complex (a) I, (b) II, (c) III, (d) IV.

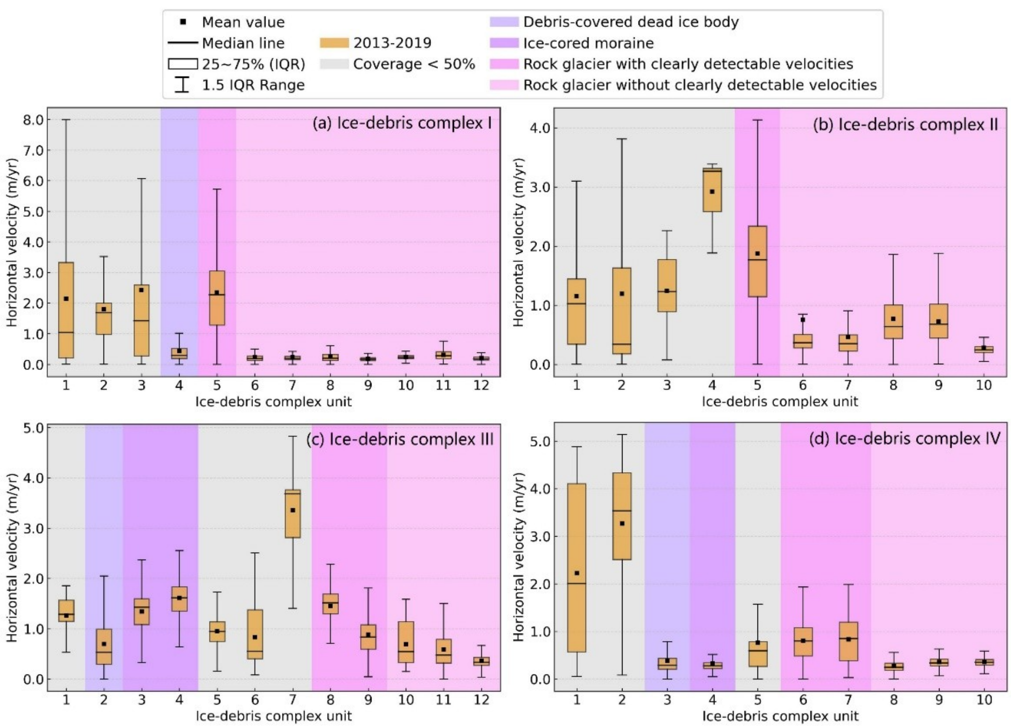

Figure 6: Distribution of horizontal velocities for ice-debris complex (a) I, (b) II, (c) III, and (d) IV in the period of 2013–2019.

https://doi.org/10.5194/egusphere-2026-3678
Preprint. Discussion started: 7 August 2026

5 Discussion

5.1 Geomorphological interpretations

The four investigated glacier-ice-debris complexes in southern Muztagh Ata can be distinguished into three distinct geomorphological domains: (1) a glacier zone, (2) a glacier-affected zone and (3) a periglacial zone (Fig. 7).

The glacier zone consists of debris-free and debris-covered glaciers. The debris-free glaciers are characterized by clean ice with supraglacial crevasses, and the debris-covered glaciers are debris-mantled in their ablation zones with the presence of supraglacial ponds, thermokarst depressions, and ice cliffs (Fig. 2). In this zone, widespread surface lowering can occur on debris-covered glaciers (I-2 and II-1) (Figs. 3a–d). However, significant elevation gains are also observed on I-1, III-1, IV-1, and IV-2 (Figs. 3a, b, e–h), which are related to glacier surging, a phenomenon well-documented in the Muztagh Ata massif (Goerlich et al., 2020; Lv et al., 2019; Guillet et al., 2022). The velocity fields in this zone contain numerous data voids (Fig. 5), likely because these glacier surfaces are either undergoing rapid melt-induced degradation or moving too rapidly for reliable feature tracking, resulting in insufficiently persistent surface features between image acquisitions.

The glacier-affected zone of ice-debris complex typically consists of ice-cored moraines and debris-covered dead ice bodies. This zone is characterized by massive ice-related features, including extensive thermokarst depressions, meltwater ponds, and supraglacial channels (Fig. 2). DEM differencing reveals substantial surface lowering at the debris-covered dead ice body units (I-4, III-2, and IV-3). The lowering rates observed in Muztagh Ata are comparable to those recorded in the Tien Shan (Bolch et al., 2019), the Central Andes of Chile and Argentina (Monnier and Kinnard, 2017; Stammler et al., 2026), and the Gruben site in the Swiss Alps (Gärtner-Roer et al., 2022; Wee et al., 2024). We interpret that this substantial volume loss is likely due to the degradation of massive buried dead ice bodies. Other units in this zone also exhibit widespread surface lowering, which likely reflects progressive melting of the ice cores preserved within ice-cored moraines.

The periglacial zone of ice-debris complexes is composed of rock glaciers showing coherent viscous flow patterns, ridge-and-furrow topography, steep frontal slopes and lateral margins (Fig. 2). The surface velocities derived from Pléiades imagery show that I-5 and II-5 exhibit velocities exceeding 6 m/yr (Fig. 5). These velocity magnitudes are much higher than the typical rock glacier velocity ranges between centimeters and one meter per year (Hu et al., 2025; Sun et al., 2025) but are comparable to the fast-moving rock glaciers in the Andes (Blöthe et al., 2025; Robson et al., 2022; Stammler et al., 2026) and Tien Shan (Kääb et al., 2021; Wood et al., 2025). The frontal elevation gains observed in these units (Fig. 3) further support active downslope creep and advance.

This geomorphological structure is in line with observations from other high-mountain regions. An upper glacier-affected zone and a lower periglacial part are also observed at Gruben and Ritord sites in the Swiss Alps (Gärtner-Roer et al., 2022; Wee et al., 2024, 2026) and the Chon-Saj and Geologov complexes in the Central Tien Shan (Bolch et al., 2019). This structure is also consistent with previously investigated landforms in the Andes, where the complexes are composed of upper debris-covered glaciers and lower rock glaciers (Monnier et al., 2014; Monnier and Kinnard, 2017; Stammler et al., 2026),

https://doi.org/10.5194/egusphere-2026-3678
Preprint. Discussion started: 7 August 2026

suggesting that the three-zone geomorphological organization identified at Muztagh Ata represents a characteristic evolutionary configuration of glacier–permafrost transitional systems.

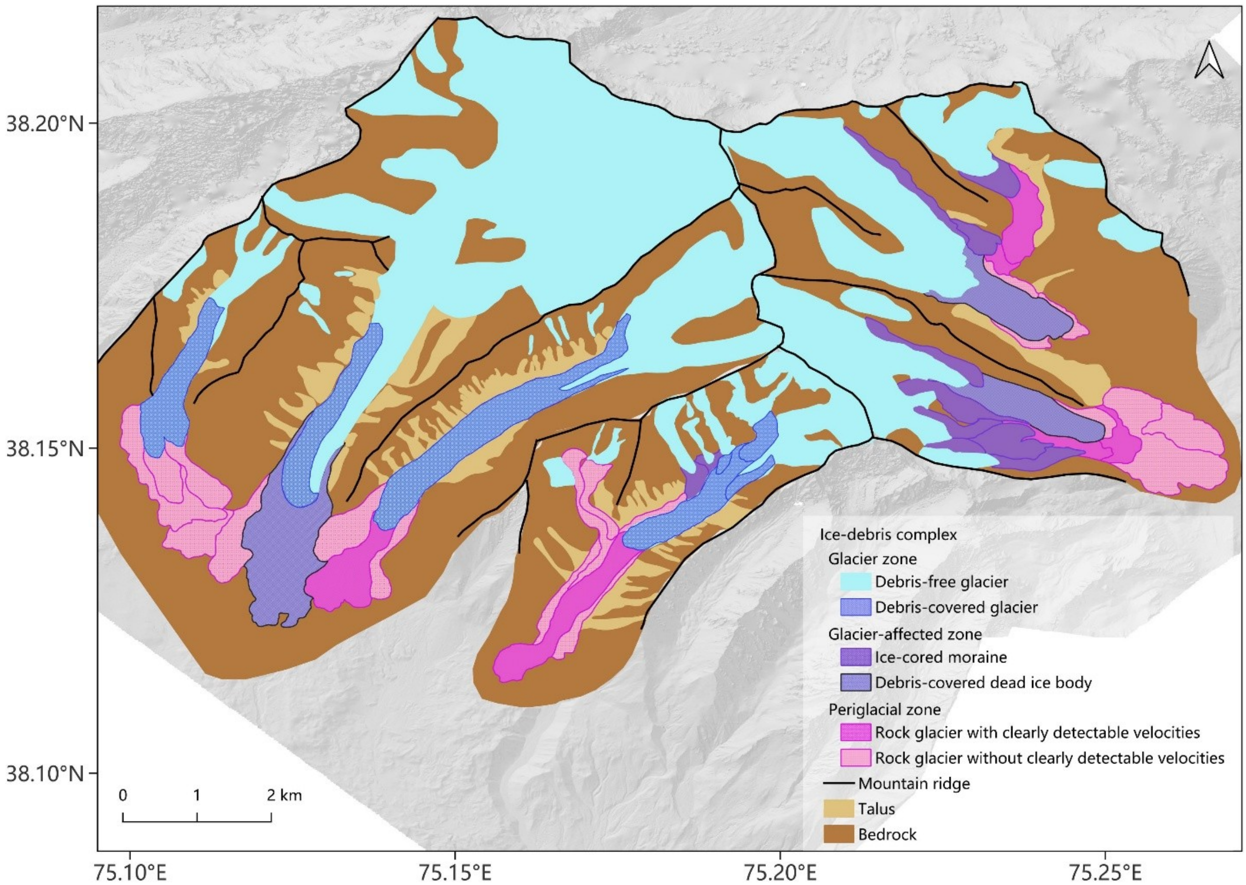

Figure 7: Geomorphological characterization of the glacier-ice-debris complexes in southern Muztagh Ata, Eastern Pamir.

5.2 Evolution of ice-debris complexes

The evolution of ice-debris complexes can generally be understood through three main processes: (i) the readvance and superimposition/embedding of debris-free/covered glaciers onto/into pre-existing rock glaciers (the "permafrost school" perspective) (Haeberli et al., 2006, 2024; Monnier et al., 2014); (ii) the continuous derivation of a rock glacier from a debris-covered glacier through the preservation and creep of a massive ice core (the "continuum school" perspective) (Anderson et al., 2018; Jones et al., 2019a); and (iii) the transformation of a debris-covered glacier into a rock glacier via the fragmentation of the glacier ice and its mixing with periglacial ice and debris (Monnier and Kinnard, 2015, 2017). Our multi-temporal remote-sensing analysis allowed us to reconstruct the long-term transitional trajectory of the ice-debris complexes in southern Muztagh Ata. According to our observations, we suggest these processes could co-exist within the same ice-debris complex system, with different components recording different stages of glacier–permafrost interaction and evolution.

https://doi.org/10.5194/egusphere-2026-3678
Preprint. Discussion started: 7 August 2026

The pronounced surface lowering observed in the debris-covered dead ice body units (I-4, III-2, and IV-3; Fig. 3) provide evidence for the "transformation" or "continuum" processes (Types ii and iii). These areas are likely to represent former glacier tongues that, once decoupled from the main accumulation area and insulated by a thick debris mantle, entered a state of thermal disequilibrium and began a slow transition toward rock glaciers under permafrost conditions (Berthling, 2011). This process is also in line with observations in the Swiss Alps (Wee et al., 2026), Tien Shan (Bolch et al., 2019), and Andes (Monnier and Kinnard, 2015, 2017; Robson et al., 2022). However, some complexes contain glacier forefields between glaciers and rock glaciers (e.g., the Chon-Saj and Geologov complexes in Tien Shan (Bolch et al., 2019) and the Complexes III and IV in this study), while others feature a more direct transition between debris-covered glaciers and glaciers (e.g., the Presenteseracae (Monnier and Kinnard, 2015, 2017) and the Las Tetas (Robson et al., 2022) in the Andes). García et al. (2024) demonstrated that the debris-covered glaciers can serve as the foundation for the development of rock glacier-like viscous flow structures under permafrost conditions based on chronological evidence.

Simultaneously, the fast-flowing rock glaciers suggest the superimposition/embedding of debris-covered glaciers onto/into rock glaciers. These debris-covered glaciers can rapidly transport massive amounts of ice and debris downslope, exerting substantial stress on downstream rock glaciers. The exceptionally high creep velocities (up to 6 m/yr) documented for I-5 and II-5 may represent a dynamic legacy of such interactions, where advancing or surging glaciers overrode or embedded glacial ice into pre-existing rock glaciers, thereby increasing the plasticity and deformation rates of the hybrid system. The observations at Gruben site in the Swiss Alps (Kääb et al., 1997; Haeberli, 2005) support this process, where both permafrost and embedded surface ice were found in the complex contact zone (Gärtner-Roer et al., 2022; Wee et al., 2024). The observations in the Andes at Tapado (Monnier et al., 2014; Robson et al., 2022) and at Navarro and Las Tetas (Monnier and Kinnard, 2017) also support this process, suggesting that rock glaciers do not derive from the present debris-covered glaciers but exist prior to them. Recent regional-scale analyses further indicate that glacier-connected rock glaciers move on average faster than talus-connected rock glaciers, suggesting that glacier-derived ice may play an important role in enhancing rock glacier surface velocities (Sun et al., 2026).

Taken together, our observations suggest that multiple evolutionary pathways can operate simultaneously within a single ice-debris complex. Rather than representing a simple linear transition from glacier to rock glacier, these complexes may evolve through repeated episodes of glacier advance, debris accumulation, dead-ice preservation, and permafrost creep, resulting in the composite geomorphological assemblages observed today.

We stress here that our findings are based on remote-sensing observations, whereas the processes responsible for debris supply, transport, and preservation remain insufficiently constrained. Fully resolving the evolutionary history will require targeted in-situ investigations, detailed geophysical surveys, and numerical modeling of debris deposition, ice melt, and coupled glacier–permafrost flow. Such work would be essential to investigate whether the present ice-debris complexes indeed represent relict debris-buried glacier remains or evolved from a more complex interplay of glacier fluctuations and permafrost creep.

https://doi.org/10.5194/egusphere-2026-3678
Preprint. Discussion started: 7 August 2026

5.3 Implications for hydrology

The DEM differences indicate substantial long-term ice loss from the ice-debris complexes. The glacier-affected and periglacial zones of the four ice-debris complexes together lost approximately 0.10 km^3 of ice during 1967–2019, including 0.09 km^3 from glacier-affected zones and 0.01 km^3 from periglacial zones. For comparison, the glacier zone is estimated to have lost approximately 0.09 km^3 of ice over the same period based on the glacier-wide volume-change estimates of Bhattacharya et al. (2021). Therefore, despite occupying a considerably smaller area than the glacier zone (15.9 km^2 versus 39.4 km^2), the glacier-affected and periglacial zones experienced a comparable amount of ice-volume loss. This result highlights the substantial ice storage preserved within ice-debris complexes and demonstrates that significant ice losses can occur beyond conventionally mapped glacier boundaries. Notably, the pronounced surface lowering in the glacier-affected zone observed in our study area results in this comparable ice volume loss, whereas in most other regions, the glacier zone is expected to dominate the total loss.

Our observations support the arguments of Janke et al. (2017) and Bolch et al. (2019) that ice-debris complexes, and particularly glacier-affected zones, represent a significant yet frequently overlooked solid water reservoirs. The abundance of rock glaciers across the Tibetan Plateau highlights the widespread occurrence and potential hydrological significance of ice-rich periglacial landforms in High Mountain Asia (Sun et al., 2024). Glacier-hydrological models (Duethmann et al., 2016; Rounce et al., 2023) generally focus on glaciers while neglecting meltwater contributions from glacier-affected and periglacial landforms. Consequently, runoff generation and long-term water availability may be underestimated in regions where ice-debris complexes are widespread. Our findings therefore emphasize the need to incorporate ice-debris complexes into glacier inventories, hydrological modelling frameworks, and regional water-resource assessments, particularly in High Mountain Asia where these landforms are abundant and may contain substantial volumes of buried ice.

6 Conclusions

This study provides the first comprehensive and long-term assessment of ice-debris complexes in the Muztagh Ata massif of the Eastern Pamir. By leveraging historical Corona KH-4A stereo imagery and contemporary Pléiades tri-stereo observations spanning from 1967 to 2019, we quantified their elevation changes, surface velocities, and geomorphological characteristics over more than five decades. Our analysis leads to the following conclusions:

1. The glacial-periglacial landform systems exhibit a three-zone geomorphological organization: (1) a glacier zone with widespread surface lowering or significant elevation gains caused by surging; (2) a glacier-affected zone dominated by thermokarst depression, supraglacial ponds, and substantial surface subsidence with maximum local lowering of 60–100 m since 1967; (3) a periglacial zone consisting of rock glaciers with peak velocities up to 6 m/yr.
2. Multiple evolutionary processes, including the transformation of glacier-affected landforms into rock glaciers and the superimposition or embedding of debris-covered glaciers onto or into pre-existing rock glaciers, can co-exist within the same ice-debris complex system. Our observations suggest that ice-debris complexes do not evolve through a single

https://doi.org/10.5194/egusphere-2026-3678
Preprint. Discussion started: 7 August 2026

linear pathway but instead record different stages of glacier–permafrost interaction operating simultaneously within a composite landform assemblage.

3. The glacier, glacier-affected, and periglacial zones occupy approximately 39.4 km^2, 6.5 km^2, and 9.4 km^2, respectively. The glacier-affected and periglacial zones together lost approximately 0.10 km^3 of ice during 1967–2019, an amount comparable to the estimated ice loss from the glacier zone despite their considerably smaller area. This finding highlights the substantial ice storage preserved within ice-debris complexes and underscores their importance as previously underappreciated solid water reservoirs.

Our analysis provides new insights into the geomorphological characteristics, evolution, and hydrological significance of ice-debris complexes in High Mountain Asia. The results further demonstrate that substantial ice losses may occur beyond conventionally mapped glacier boundaries, emphasizing the need to incorporate ice-debris complexes into inventories, hydrological models, and regional water-resource assessments. Future research integrating geophysical surveys, subsurface characterization, and numerical modelling will be essential to fully resolve their internal structures, ice content, and evolutionary trajectories.

Code and data availability

The Corona KH-4A data can be downloaded from USGS archive (https://earthexplorer.usgs.gov/). The Ames Stereo Pipeline package is available at https://github.com/NeoGeographyToolkit/StereoPipeline. The xDEM package is available at https://xdem.readthedocs.io/en/stable/. The vmap package is available at https://github.com/dshean/vmap. The elevation change, surface velocity, and unit boundary data of the ice-debris complexes generated from this study are available at https://doi.org/10.5281/zenodo.20351004.

Author contributions

Zhangyu Sun: Data curation, Formal analysis, Investigation, Methodology, Visualization, Writing – original draft, Writing – review and editing. **Tobias Bolch:** Conceptualization, Project management, Methodology, Resources, Supervision, Writing – review and editing. **Daniel Falaschi:** Methodology, Writing – review and editing. **Atanu Bhattacharya:** Investigation, Methodology, Writing – review and editing. **Lin Liu:** Resources, Supervision, Writing – review and editing.

Competing interests

Some authors are members of the editorial board of The Cryosphere.

https://doi.org/10.5194/egusphere-2026-3678
Preprint. Discussion started: 7 August 2026

Disclaimer

Acknowledgements

This work was supported by the Hong Kong Research Grants Council (HKPFS PF20-42392), the CUHK–Exeter Joint Centre for Environmental Sustainability and Resilience (ENSURE, grant no. 4930821), and the Federal Ministry of Education, Science and Research, Austria's Agency for Education and Internationalization (MPC-2023-00719). We acknowledge CNES and Airbus Defence and Space for the provision of the Pléiades data at a reduced cost through the ISIS project (© CNES and Airbus DS, 2013, 2019, all rights reserved)

References

Anderson, R. S., Anderson, L. S., Armstrong, W. H., Rossi, M. W., and Crump, S. E.: Glaciation of alpine valleys: The glacier–debris-covered glacier–rock glacier continuum, Geomorphology, 351, 127–142, https://doi.org/10.1016/j.geomorph.2018.03.015, 2018.

Belart, J. M. C., Berthier, E., Magnússon, E., Anderson, L. S., Pálsson, F., Thorsteinsson, T., Howat, I. M., Aðalgeirsdóttir, G., Jóhannesson, T., and Jarosch, A. H.: Winter mass balance of Drangajökull ice cap (NW Iceland) derived from satellite sub-meter stereo images, The Cryosphere, 11, 1501–1517, https://doi.org/10.5194/tc-11-1501-2017, 2017.

Berthier, E. and Brun, F.: Karakoram geodetic glacier mass balances between 2008 and 2016: persistence of the anomaly and influence of a large rock avalanche on Siachen Glacier, J. Glaciol., 65, 494–507, https://doi.org/10.1017/jog.2019.32, 2019.

Berthier, E., Lebreton, J., Fontannaz, D., Hosford, S., Belart, J. M.-C., Brun, F., Andreassen, L. M., Menounos, B., and Blondel, C.: The Pléiades Glacier Observatory: High-resolution digital elevation models and ortho-imagery to monitor glacier change, The Cryosphere, 18, 5551–5571, https://doi.org/10.5194/tc-18-5551-2024, 2024.

Berthling, I.: Beyond confusion: Rock glaciers as cryo-conditioned landforms, Geomorphology, 131, 98–106, https://doi.org/10.1016/j.geomorph.2011.05.002, 2011.

Bhattacharya, A., Bolch, T., Mukherjee, K., King, O., Menounos, B., Kapitsa, V., Neckel, N., Yang, W., and Yao, T.: High Mountain Asian glacier response to climate revealed by multi-temporal satellite observations since the 1960s, Nat. Commun., 12, 4133, https://doi.org/10.1038/s41467-021-24180-y, 2021.

https://doi.org/10.5194/egusphere-2026-3678
Preprint. Discussion started: 7 August 2026

Blöthe, J. H., Falaschi, D., Vivero, S., and Tadono, T.: Rock glacier kinematics in the Valles Calchaquíes Region, Northwestern Argentina, from multi-temporal aerial and satellite imagery (1968–2023), Permafr. Periglac. Process., 36, 123–136, https://doi.org/10.1002/ppp.2260, 2025.

Blöthe, J. H., Halla, C., Schwalbe, E., Bottegal, E., Trombotto Liaudat, D., and Schrott, L.: Surface velocity fields of active rock glaciers and ice-debris complexes in the Central Andes of Argentina, Earth Surf. Process. Landf., 46, 504–522, https://doi.org/10.1002/esp.5042, 2021.

Bolch, T., Rohrbach, N., Kutuzov, S., Robson, B. A., and Osmonov, A.: Occurrence, evolution and ice content of ice-debris complexes in the Ak-Shiirak, Central Tien Shan revealed by geophysical and remotely-sensed investigations, Earth Surf. Process. Landf., 44, 129–143, https://doi.org/10.1002/esp.4487, 2019.

Brardinoni, F., Vivero, S., Barboux, C., Bodin, X., Cicoira, A., Echelard, T., Hu, Y., Jones, N., Lambiel, C., MacDonell, S., Pellet, C., Rouyet, L., Ruiz, L., Schaffer, N., Wehbe, M., and Delaloye, R.: RGIK guidelines for compiling consistent rock glacier inventories, Geomorphology, 492, 110050, https://doi.org/10.1016/j.geomorph.2025.110050, 2026.

Cusicanqui, D., Rabatel, A., Vincent, C., Bodin, X., Thibert, E., and Francou, B.: Interpretation of volume and flux changes of the Laurichard rock glacier between 1952 and 2019, French Alps, J. Geophys. Res. Earth Surf., 126, e2021JF006161, https://doi.org/10.1029/2021JF006161, 2021.

Dehecq, A., Millan, R., Berthier, E., Gourmelen, N., Trouve, E., and Vionnet, V.: Elevation changes inferred from TanDEM-X data over the Mont-Blanc area: Impact of the X-band interferometric bias, IEEE J. Sel. Top. Appl. Earth Obs. Remote Sens., 9, 3870–3882, https://doi.org/10.1109/JSTARS.2016.2581482, 2016.

Duethmann, D., Menz, C., Jiang, T., and Vorogushyn, S.: Projections for headwater catchments of the Tarim River reveal glacier retreat and decreasing surface water availability but uncertainties are large, Environ. Res. Lett., 11, 054024, https://doi.org/10.1088/1748-9326/11/5/054024, 2016.

European Space Agency: Copernicus Global Digital Elevation Model, Distributed by OpenTopography [data set], https://doi.org/10.5069/G9028PQB, 2024.

Falaschi, D., Bhattacharya, A., Guillet, G., Huang, L., King, O., Mukherjee, K., Pieczonka, T., and Bolch, T.: Annual to seasonal glacier mass balance in High Mountain Asia derived from Pléiades stereo images: examples from the Pamir and the Tibetan Plateau, The Cryosphere, 17, 5435–5458, https://doi.org/10.5194/tc-17-5435-2023, 2023.

García, J. L., Carraha, J., Fernández-Navarro, H., Nussbaumer, S. U., Pérez, F., Hidy, A. J., Villarroel, C. D., and Haeberli, W.: Glacial to periglacial transition at the end of the last ice age in the subtropical semiarid Andes, Geomorphology, 465, 109379, https://doi.org/10.1016/j.geomorph.2024.109379, 2024.

Gärtner-Roer, I., Brunner, N., Delaloye, R., Haeberli, W., Kääb, A., and Thee, P.: Glacier–permafrost relations in a high-mountain environment: 5 decades of kinematic monitoring at the Gruben site, Swiss Alps, The Cryosphere, 16, 2083–2101, https://doi.org/10.5194/tc-16-2083-2022, 2022.

https://doi.org/10.5194/egusphere-2026-3678
Preprint. Discussion started: 7 August 2026

Goerlich, F., Bolch, T., Mukherjee, K., and Pieczonka, T.: Glacier mass loss during the 1960s and 1970s in the Ak-Shirak range (Kyrgyzstan) from multiple stereoscopic Corona and Hexagon imagery, Remote Sens., 9, 275, https://doi.org/10.3390/rs9030275, 2017.

Goerlich, F., Bolch, T., and Paul, F.: More dynamic than expected: an updated survey of surging glaciers in the Pamir, Earth Syst. Sci. Data, 12, 3161–3180, https://doi.org/10.5194/essd-12-3161-2020, 2020.

Grodecki, J. and Dial, G.: Block adjustment of high-resolution satellite images described by rational polynomials, Photogramm. Eng. Remote Sens., 69, 59–68, https://doi.org/10.14358/PERS.69.1.59, 2003.

Gruber, S.: Derivation and analysis of a high-resolution estimate of global permafrost zonation, The Cryosphere, 6, 221–233, https://doi.org/10.5194/tc-6-221-2012, 2012.

Guillet, G., King, O., Lv, M., Ghuffar, S., Benn, D., Quincey, D., and Bolch, T.: A regionally resolved inventory of High Mountain Asia surge-type glaciers, derived from a multi-factor remote sensing approach, The Cryosphere, 16, 603–623, https://doi.org/10.5194/tc-16-603-2022, 2022.

Haeberli, W.: Investigating glacier–permafrost relationships in high mountain areas: historical background, selected examples and research needs, in: Cryospheric Systems: Glaciers and Permafrost, edited by: Harris, C. and Murton, J. B., Geol. Soc. Lond. Spec. Publ., 242, 29–37, https://doi.org/10.1144/GSL.SP.2005.242.01.03, 2005.

Haeberli, W., Arenson, L. U., Wee, J., Hauck, C., and Mölg, N.: Discriminating viscous-creep features (rock glaciers) in mountain permafrost from debris-covered glaciers – a commented test at the Gruben and Yerba Loca sites, Swiss Alps and Chilean Andes, The Cryosphere, 18, 1669–1683, https://doi.org/10.5194/tc-18-1669-2024, 2024.

Haeberli, W., Hallet, B., Arenson, L., Elconin, R., Humlum, O., Kääb, A., Kaufmann, V., Ladanyi, B., Matsuoka, N., Springman, S., and Mühll, D. V.: Permafrost creep and rock glacier dynamics, Permafr. Periglac. Process., 17, 189–214, https://doi.org/10.1002/ppp.561, 2006.

Harrison, S., Jones, D., Anderson, K., Shannon, S., and Betts, R. A.: Is ice in the Himalayas more resilient to climate change than we thought?, Geogr. Ann. A, 103, 1–7, https://doi.org/10.1080/04353676.2021.1888202, 2021.

Harrison, S., Jones, D. B., Racoviteanu, A. E., Anderson, K., Shannon, S., Betts, R. A., and Leng, R.: Rock glacier distribution across the Himalaya, Global Planet. Change, 239, 104481, https://doi.org/10.1016/j.gloplacha.2024.104481, 2024.

Harrison, S., Racoviteanu, A., Shannon, S., Jones, D., Anderson, K., Glasser, N., Knight, J., Ranger, A., Mandal, A., Vishwakarma, B. D., Kargel, J. S., Shugar, D., Haritashya, U., Li, D., Koutroulis, A., Wyser, K., and Inglis, S.: Will landscape responses reduce glacier sensitivity to climate change in High Mountain Asia?, The Cryosphere, 19, 4113–4124, https://doi.org/10.5194/tc-19-4113-2025, 2025.

Herreid, S. and Pellicciotti, F.: The state of rock debris covering Earth's glaciers, Nat. Geosci., 13, 621–627, https://doi.org/10.1038/s41561-020-0615-0, 2020.

Hirschmüller, H.: Stereo processing by semiglobal matching and mutual information, IEEE Trans. Pattern Anal. Mach. Intell., 30, 328–341, https://doi.org/10.1109/TPAMI.2007.1166, 2008.

https://doi.org/10.5194/egusphere-2026-3678
Preprint. Discussion started: 7 August 2026

Höhle, J. and Höhle, M.: Accuracy assessment of digital elevation models by means of robust statistical methods, ISPRS J. Photogramm. Remote Sens., 64, 398–406, https://doi.org/10.1016/j.isprsjprs.2009.02.003, 2009.

Holzer, N., Vijay, S., Yao, T., Xu, B., Buchroithner, M., and Bolch, T.: Four decades of glacier variations at Muztagh Ata (eastern Pamir): a multi-sensor study including Hexagon KH-9 and Pléiades data, The Cryosphere, 9, 2071–2088, https://doi.org/10.5194/tc-9-2071-2015, 2015.

Hu, Y., Arenson, L. U., Barboux, C., Bodin, X., Cicoira, A., Delaloye, R., Gärtner-Roer, I., Kääb, A., Kellerer-Pirklbauer, A., Lambiel, C., Liu, L., Pellet, C., Rouyet, L., Schoeneich, P., Seier, G., and Strozzi, T.: Rock Glacier Velocity: An Essential Climate Variable Quantity for Permafrost, Rev. Geophys., 63, e2024RG000847, https://doi.org/10.1029/2024RG000847, 2025.

Hugonnet, R., Mannerfelt, E., Dehecq, A., Dubois, E., De Bardonnèche-Richard, A., Schaffner, V., Knuth, F., Froessl, A., Liu, Z., Tedstone, A., Landmann, J. M., McNabb, R., Mattea, E., Cusicanqui, D., Schenck, F., and Gentilini, A.: xDEM (v0.0.18), Zenodo [code], https://doi.org/10.5281/zenodo.11204531, 2024.

Hugonnet, R., McNabb, R., Berthier, E., Menounos, B., Nuth, C., Girod, L., Farinotti, D., Huss, M., Dussaillant, I., Brun, F., and Kääb, A.: Accelerated global glacier mass loss in the early twenty-first century, Nature, 592, 726–731, https://doi.org/10.1038/s41586-021-03436-z, 2021.

Janke, J. R., Ng, S., and Bellisario, A.: An inventory and estimate of water stored in firn fields, glaciers, debris-covered glaciers, and rock glaciers in the Aconcagua River Basin, Chile, Geomorphology, 296, 142–152, https://doi.org/10.1016/j.geomorph.2017.09.002, 2017.

Jones, D. B., Harrison, S., and Anderson, K.: Mountain glacier-to-rock glacier transition, Global Planet. Change, 181, 102999, https://doi.org/10.1016/j.gloplacha.2019.102999, 2019a.

Jones, D. B., Harrison, S., Anderson, K., and Whalley, W. B.: Rock glaciers and mountain hydrology: A review, Earth-Sci. Rev., 193, 66–90, https://doi.org/10.1016/j.earscirev.2019.04.001, 2019b.

Kääb, A., Haeberli, W., and Gudmundsson, G.: Analysing the creep of mountain permafrost using high precision aerial photogrammetry: 25 years of monitoring Gruben rock glacier, Swiss Alps, Permafr. Periglac. Process., 8, 409–426, https://doi.org/10.1002/(SICI)1099-1530(199710/12)8:4<409::AID-PPP267>3.0.CO;2-C, 1997.

Kääb, A., Strozzi, T., Bolch, T., Caduff, R., Trefall, H., Stoffel, M., and Kokarev, A.: Inventory and changes of rock glacier creep speeds in Ile Alatau and Kungöy Ala-Too, northern Tien Shan, since the 1950s, The Cryosphere, 15, 927–944, https://doi.org/10.5194/tc-15-927-2021, 2021.

Kääb, A., Treichler, D., Nuth, C., and Berthier, E.: Brief Communication: Contending estimates of 2003–2008 glacier mass balance over the Pamir–Karakoram–Himalaya, The Cryosphere, 9, 557–564, https://doi.org/10.5194/tc-9-557-2015, 2015.

Knight, J. and Harrison, S.: Glacial and paraglacial environments, Geogr. Ann. Ser. A Phys. Geogr., 96, 241–244, https://doi.org/10.1144/SP320, 2014.

Lambiel, C., Maillard, B., Kummert, M., and Reynard, E.: Geomorphology of the Hérens valley (Swiss Alps), J. Maps, 12, 160–172, https://doi.org/10.1080/17445647.2014.999135, 2016.

Lambiel, C., Maillard, B., Martin, S., Pellitero Ondicol, R., Schoeneich, P., and Reynard, E.: Adaptation of the geomorphological mapping system of the University of Lausanne for ArcGIS, in: Proceedings of the 8th International Conference on Geomorphology, Paris, France, 27–31 August 2013, 2013.

Lugon, R. and Stoffel, M.: Rock-glacier dynamics and magnitude–frequency relations of debris flows in a high-elevation watershed: Ritigraben, Swiss Alps, Global Planet. Change, 73, 202–210, https://doi.org/10.1016/j.gloplacha.2010.06.004, 2010.

Lv, M., Guo, H., Lu, X., Liu, G., Yan, S., and Ruan, Z.: Characterizing the behaviour of surge-and non-surge-type glaciers in the Kingata Mountains, eastern Pamir, from 1999 to 2016, The Cryosphere, 13, 219–236, https://doi.org/10.5194/tc-13-219-2019, 2019.

Lv, M., Quincey, D. J., Guo, H., King, O., Liu, G., Yan, S., Lu, X., and Ruan, Z.: Examining geodetic glacier mass balance in the eastern Pamir transition zone, J. Glaciol., 66, 927–937, https://doi.org/10.1017/jog.2020.54, 2020.

Monnier, S. and Kinnard, C.: Internal structure and composition of a rock glacier in the dry Andes, inferred from ground-penetrating radar data and its artefacts, Permafr. Periglac. Process., 26, 335–346, https://doi.org/10.1002/ppp.1846, 2015.

Monnier, S. and Kinnard, C.: Pluri-decadal (1955–2014) evolution of glacier–rock glacier transitional landforms in the central Andes of Chile (30–33° S), Earth Surf. Dyn., 5, 493–509, https://doi.org/10.5194/esurf-5-493-2017, 2017.

Monnier, S., Kinnard, C., Surazakov, A. B., and Bossy, W.: Geomorphology, internal structure, and successive development of a glacier foreland in the semiarid Chilean Andes (Cerro Tapado, upper Elqui Valley, 30°08′ S., 69°55′ W.), Geomorphology, 207, 126–140, https://doi.org/10.1016/j.geomorph.2015.02.010, 2014.

Munroe, J. S., Laabs, B. J., Corbett, L. B., Bierman, P. R., and Handwerger, A. L.: Rock glacier movement and debris transport over annual to multi-millennial timescales, J. Geophys. Res. Earth Surf., 129, e2023JF007453, https://doi.org/10.1029/2023JF007453, 2024.

Nefian, A. V., Husmann, K., Broxton, M., To, V., Lundy, M., and Hancher, M. D.: A Bayesian formulation for sub-pixel refinement in stereo orbital imagery, 2009 16th IEEE Int. Conf. Image Process. (ICIP), 2361–2364, https://doi.org/10.1109/ICIP.2009.5413749, 2009.

Nuth, C. and Kääb, A.: Co-registration and bias corrections of satellite elevation data sets for quantifying glacier thickness change, The Cryosphere, 5, 271–290, https://doi.org/10.5194/tc-5-271-2011, 2011.

Paul, F., Winsvold, S. H., Kääb, A., Nagler, T., and Schwaizer, G.: Glacier remote sensing using Sentinel-2. Part II: Mapping glacier extents and surface facies, and comparison to Landsat 8, Remote Sens., 8, 575, https://doi.org/10.3390/rs8070575, 2016.

RGI 7.0 Consortium: Randolph Glacier Inventory - A Dataset of Global Glacier Outlines, Version 7.0, NSIDC: National Snow and Ice Data Center [data set], https://doi.org/10.5067/f6jmovy5navz, 2023.

Robson, B. A., MacDonell, S., Ayala, Á., Bolch, T., Nielsen, P. R., and Vivero, S.: Glacier and rock glacier changes since the 1950s in the La Laguna catchment, Chile, The Cryosphere, 16, 647–665, https://doi.org/10.5194/tc-16-647-2022, 2022.

Rounce, D. R., Hock, R., Maussion, F., Hugonnet, R., Kochtitzky, W., Huss, M., Berthier, E., Brinkerhoff, D., Compagno, L., Copland, L., Farinotti, D., FitzGerald, J. J., Jakobs, N., Kraaijenbrink, P. D. A., Prins, R. B., Reggane, A. J., Veldhuijsen, S. B. M., Westermann, S., and McNabb, R. W.: Global glacier change in the 21st century: Every increase in temperature matters, Science, 379, 78–83, https://doi.org/10.1126/science.abo1324, 2023.

Scheffler, D., Hollstein, A., Diedrich, H., Segl, K., and Hostert, P.: AROSICS: An Automated and Robust Open-Source Image Co-Registration Software for Multi-Sensor Satellite Data, Remote Sens., 9, 676, https://doi.org/10.3390/rs9070676, 2017.

Shean, D. E., Alexandrov, O., Moratto, Z. M., Smith, B. E., Joughin, I. R., Porter, C., and Morin, P.: An automated, open-source pipeline for mass production of digital elevation models (DEMs) from very-high-resolution commercial stereo satellite imagery, ISPRS J. Photogramm. Remote Sens., 116, 101–117, https://doi.org/10.1016/j.isprsjprs.2016.03.012, 2016.

Shean, D. E., Bhushan, S., Montesano, P., Rounce, D. R., Arendt, A., and Osmanoglu, B.: A systematic, regional assessment of high mountain Asia glacier mass balance, Front. Earth Sci., 7, 363, https://doi.org/10.3389/feart.2019.00363, 2020.

Sohn, H. G., Kim, G. H., and Yom, J. H.: Mathematical modelling of historical reconnaissance CORONA KH-4B imagery, Photogramm. Rec., 19, 51–66, https://doi.org/10.1046/j.0031-868X.2003.00257.x, 2004.

Stammler, M., Blöthe, J., Cusicanqui, D., Ebert, S., Bell, R., Bodin, X., and Schrott, L.: Glacial decline next to stable permafrost in the Dry Andes? Vertical glacier surface changes and rock glacier kinematics based on Pléiades imagery (Rodeo basin, 2019–2025), The Cryosphere, 20, 2257–2277, https://doi.org/10.5194/tc-20-2257-2026, 2026.

Sun, Z., Hu, Y., Racoviteanu, A., Liu, L., Harrison, S., Wang, X., Cai, J., Guo, X., He, Y., and Yuan, H.: TPRoGI: a comprehensive rock glacier inventory for the Tibetan Plateau using deep learning, Earth Syst. Sci. Data, 16, 5703–5721, https://doi.org/10.5194/essd-16-5703-2024, 2024.

Sun, Z., Liu, L., and Bolch, T.: Uncovering controlling factors on rock glacier velocities in the Pamir–Karakoram–Kunlun region using explainable machine learning, PNAS Nexus, 5, pgag177, https://doi.org/10.1093/pnasnexus/pgag177, 2026.

Sun, Z., Liu, L., Fan, C., Hu, Y., Baldacchino, F., Bhattacharya, A., Wood, E., and Bolch, T.: Unveiling large-scale velocity characteristics of rock glaciers in the Tibet-Pamir-Karakoram region using InSAR, Int. J. Appl. Earth Obs. Geoinf., 142, 104733, https://doi.org/10.1016/j.jag.2025.104733, 2025.

Villarroel, C. D., Ortiz, D. A., Forte, A. P., Tamburini Beliveau, G., Ponce, D., Imhof, A., and López, A.: Internal structure of a large, complex rock glacier and its significance in hydrological and dynamic behavior: A case study in the semi-arid Andes of Argentina, Permafr. Periglac. Process., 33, 78–95, https://doi.org/10.1002/ppp.2132, 2022.

Wee, J., Hendrickx, H., and Vivero, S.: Capturing the multi-decadal evolution of glacier–permafrost interactions in a high-alpine environment (Ritord, western Swiss Alps), Permafr. Periglac. Process., https://doi.org/10.1002/ppp.70043, 2026.

https://doi.org/10.5194/egusphere-2026-3678
Preprint. Discussion started: 7 August 2026

Wee, J., Vivero, S., Mathys, T., Mollaret, C., Hauck, C., Lambiel, C., and Haeberli, W.: Characterizing ground ice content and origin to better understand the seasonal surface dynamics of the Gruben rock glacier and the adjacent Gruben debris-covered glacier (southern Swiss Alps), The Cryosphere, 18, 5939–5963, https://doi.org/10.5194/tc-18-5939-2024, 2024.

Wood, E., Bolch, T., Kapitsa, V., Baldacchino, F., Blagoveshchensky, V., Rahimov, F., Taskynbayev, A., and Schrott, L.: Deciphering transitions within ice–debris complexes in the Northern Tien Shan through surface characteristics and internal structure, Earth Surf. Process. Landf., 51, e70309, https://doi.org/10.1002/esp.70309, 2026.

Wood, E., Bolch, T., and Streeter, R.: Insights from feature tracking of optical satellite data for studying rock glacier kinematics in the Northern Tien Shan, Front. Earth Sci., 12, 1518390, https://doi.org/10.3389/feart.2024.1518390, 2025.

Yang, Y., Li, Z., Wang, F., Zhao, W., Mu, J., Jin, S., and Ma, H.: Ice thickness measurement and volume modeling of Muztagh Ata Glacier No. 16, Eastern Pamir, Remote Sens., 16, 2009, https://doi.org/10.3390/rs16112009, 2024.

Zalazar, L., Ferri, L., Castro, M., Gargantini, H., Gimenez, M., Pitte, P., Ruiz, L., Masiokas, M., Costa, G., and Villalba, R.: Spatial distribution and characteristics of Andean ice masses in Argentina: results from the first National Glacier Inventory, J. Glaciol., 66, 938–949, https://doi.org/10.1017/jog.2020.55, 2020.

Zhou, J., Li, Z., and Guo, W.: Estimation and analysis of the surface velocity field of mountain glaciers in Muztag Ata using satellite SAR data, Environ. Earth Sci., 71, 3581–3592, https://doi.org/10.1007/s12665-013-2749-5, 2014.

Zhou, Y., Li, G. Y., Jin, H. J., Marchenko, S. S., Ma, W., Du, Q. S., and Chen, D.: Viscous creep of ice-rich permafrost debris in a recently uncovered proglacial area in the Tianshan Mountains, China, Adv. Clim. Change Res., 13, 540–553, https://doi.org/10.1016/j.accre.2022.05.005, 2022.